UCLA
UCLA Previously Published Works

Title
Nanostructured Fibrous Membranes with Rose Spike-Like Architecture.

Permalink

Journal

ISSN

Authors
Nasajpour, Amir
Mandla, Serena
Shree, Sindu
et al.

Publication Date

DOI

Peer reviewed

Nanostructured Fibrous Membranes with Rose Spike-Like Architecture

Amir Nasajpour,[†,‡] Serena Mandla,[†,‡] Sindu Shree,[§] Ebrahim Mostafavi,[∥] Roholah Sharifi,[†,‡]
Akbar Khalilpour,[†,‡] Saghi Saghazadeh,[†,‡] Shabir Hassan,[†,‡] Michael J. Mitchell,[⊥,#]
Jeroen Leijten,[†,‡,▽] Xu Hou,[¶] Alireza Moshaverinia,[□] Nasim Annabi,[†,‡,∥] Rainer Adelung,[§]
Yogendra Kumar Mishra,[§] Su Ryon Shin,*[●,■] Ali Tamayol,*[●,■,○] and Ali Khademhosseini*[●,■,●,△]

[†]Biomaterials Innovation Research Center, Division of Biomedical Engineering, Department of Medicine, Brigham and Women's Hospital, Harvard Medical School, Cambridge, Massachusetts 02139, United States

[‡]Harvard−MIT Division of Health Sciences and Technology, Massachusetts Institute of Technology, Cambridge, Massachusetts 02139, United States

[§]Institute for Materials Science, Kiel University, Kaiserstraße 2, D-24143 Kiel, Germany

[∥]Department of Chemical Engineering, Northeastern University, Boston, Massachusetts 02115-5000, United States

[⊥]Department of Bioengineering, University of Pennsylvania, Philadelphia, Pennsylvania 19104, United States

[#]Department of Chemical Engineering, David H. Koch Institute for Integrative Cancer Research, Massachusetts Institute of Technology, Cambridge, Massachusetts 02139, United States

[▽]Department of Developmental BioEngineering, MIRA Institute for Biomedical Technology and Technical Medicine, University of Twente, Drienerlolaan 5, 7522 NB Enschede, The Netherlands

[¶]State Key Laboratory of Physical Chemistry of Solid Surface, Collaborative Innovation Center of Chemistry for Energy Materials, College of Chemistry and Chemical Engineering, Xiamen University, Xiamen 361005, China

[□]Weintraub Center for Reconstructive Biotechnology Division of Advanced Prosthodontics, School of Dentistry, University of California, Los Angeles, California 90095, United States

[■]Wyss Institute for Biologically Inspired Engineering, Harvard University, Boston, Massachusetts 02115, United States

[○]Department of Mechanical and Materials Engineering, University of Nebraska, Lincoln, Nebraska 68588, United States

[●]Department of Bioindustrial Technologies, College of Animal Bioscience and Technology, Konkuk University, Seoul, 143-701, The Republic of Korea

[△]Center of Nanotechnology, King Abdulaziz University, Jeddah 21569, Saudi Arabia

Ⓢ Supporting Information

ABSTRACT: Nanoparticles have been used for engineering composite materials to improve the intrinsic properties and/or add functionalities to pristine polymers. The majority of the studies have focused on the incorporation of spherical nanoparticles within the composite fibers. Herein, we incorporate anisotropic branched-shaped zinc oxide (ZnO) nanoparticles into fibrous scaffolds fabricated by electrospinning. The addition of the branched particles resulted in their protrusion from fibers, mimicking the architecture of a rose stem. We demonstrated that the encapsulation of different-shape particles significantly influences the physicochemical and biological activities of the resultant composite scaffolds. In particular, the branched nanoparticles induced heterogeneous crystallization of the polymeric matrix and enhance the ultimate mechanical strain and strength. Moreover, the three-dimensional (3D) nature of the branched ZnO nanoparticles enhanced adhesion properties of the composite scaffolds to the tissues. In addition, the rose stem-like constructs offered excellent antibacterial activity, while supporting the growth of eukaryote cells.

KEYWORDS: Branched tetrapod nanoparticles, zinc oxide, electrospinning, nanocomposites, antimicrobial, scaffolds
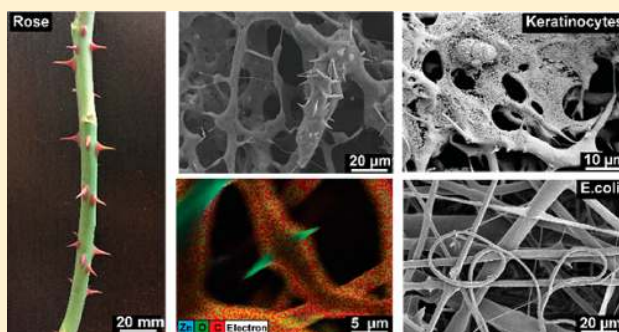
P olymeric nanocomposites are widely processed into fibrous materials for various disciplines such as tissue engineering,[1,2] energy harvesting,[3] flexible electronics,[4] drug delivery,[5] and methods of filtration.[6] Generally, some nanoscale structures from

inorganic materials, e.g., from metals, metal oxides, are dispersed into polymer structures to provide additional chemical and/or physical functionalities.[7,8] Previous works of spherical zinc oxide (ZnO) nanoparticles dispersed within semicrystalline polycaprolactone (PCL) fibrous structures have demonstrated enhancements in antimicrobial activities,[9] angiogenesis in vivo,[10] and dermal regeneration.[11] However, the recent advances in nanomaterial synthesis allow the production of a new class of branched ZnO nanoparticles via the flame transport synthesis technique.[12] The unique branched geometry of this nanomaterial allows the creation of physical interlocking segments, which provides diverse functionalities in the field of self-reporting materials,[13] antifouling surfaces,[14] electronic sensing devices,[15] gene transfection agents,[16] and antiviral materials,[17] as well as bonding to nonadherent surfaces.[18] In this work, flame-made branched ZnO nanostructures (spikes length in the 1−5 μm range and diameters in the 50−200 nm range, as confirmed by scanning electron microscopy images shown in Figures S1 and S2) were incorporated into the PCL scaffold via electrospinning. We studied the physical and chemical properties of engineered composites as compared to pristine PCL and electrospun PCL scaffold embedded with spherical particles. Due to the irregular shape of the branched ZnO particles, these nanostructures could not be fully confined into the fibers, resulting in protrusions from fibers' surfaces. Such protrusions mimic the natural structure of rose spikes. As reported by Zander et al., nanosized spikes increase the roughness and surface area of the material and affect the overall chemical and physical properties of the resultant hybrid structures.[19] In this study, we investigated the effects of particle geometry on the physical, chemical, and biological properties of the composite fibers by manipulating particle-fiber interphase.

Spherical and branched ZnO particles were dispersed in a 10% (w/v) solution of PCL in hexafluoroisopropanol (HFIP) and electrospun to obtain fibrous composite scaffolds. Pristine PCL fibrous scaffolds were also prepared. The strong particle−polymer interactions between ZnO and PCL inhibited phase separation during the solvent evaporation.[20] The scanning electron microscopy (SEM) images of the branched composite scaffold illustrated that the nanostructures were not totally confined within the fibers, showing branching protrusions through the fibers' surfaces, mimicking the rose spikes architecture (Figure 1a and Figure S1). The surface of the spherical-particle encapsulated nanofibers on the other hand appeared to be just slightly rough at the fiber interphase while the pristine PCL fibrous surface was smooth (Supporting Information S1A). Higher branched particle fractions (3 and 5% w/v) led to an overlapping of the protrusions, forming macropores within the fibrous substrates (Figure S4). Energy dispersive X-ray microanalysis (EDX) was deployed and merged with the SEM analysis to map the elemental atoms and to identify the particle distribution within the fibrous networks. The highest distribution of zinc atoms on the fiber surface was visible on constructs with spherical particles, which was proportional to the nanomaterial concentration. This evidence was related to the greater surface-area-to-volume ratio of the spherical nanoparticles as compared to the branched particles (considering equal weight per volume ratio) (Figure 1b).

Fourier transform infrared spectroscopy (FTIR) analysis was performed to identify the variations in the particle−polymer
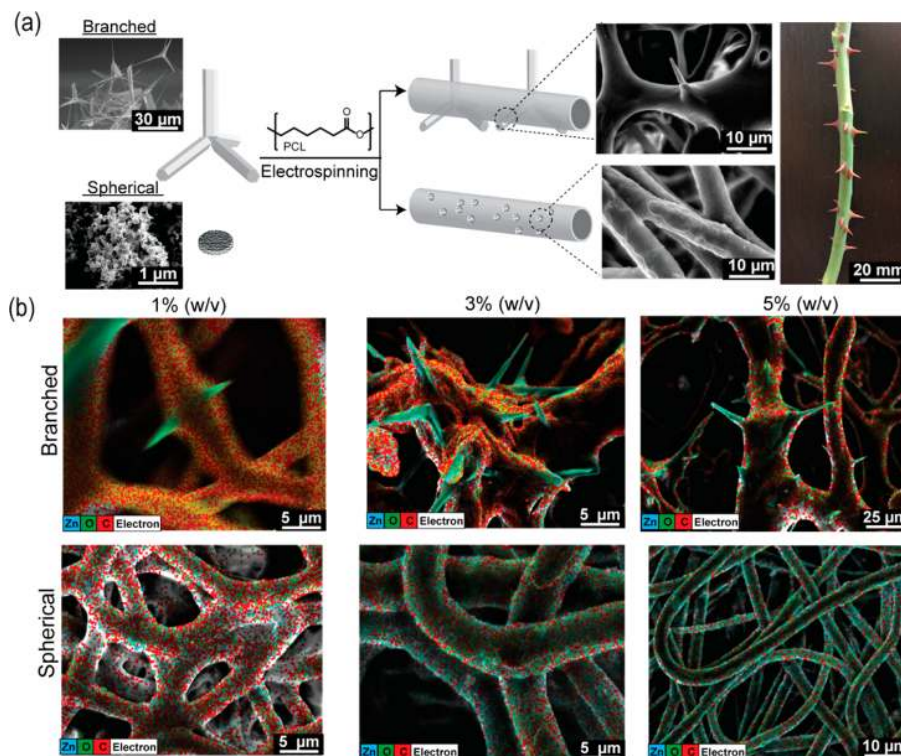

Figure 1. Fabrication of the rose stem-like composite constructs containing spherical and branched nanoparticles. (a) Schematic illustration of fibrous composite fabrication: ZnO particles are dispersed within a PCL solution and extruded under high voltage. SEM images show the inability to confine the branched particle with consequent protrusion formation (rose stem-like structure). (b) EDAX map of dibranched and spherical ZnO particles at different concentrations (1, 3, and 5% w/v) and their distribution into the fibers. Elemental map demonstrates the distribution of Zn (blue), O (green), and C (red) in the composites.

interphase interactions induced by the geometrical nature of the nanomaterials[21] (Figure 2a, c). As shown in Figure 2a, the carbonyl peaks [ν(C=O)] of pristine PCL and spherical-particle incorporated fibrous materials appeared at 1716 cm^{-1} while for the branched system the peak shifted to a lower wavenumber (1714 cm^{-1}). Moreover, the asymmetrical ester peak of branched composite scaffold was also shifted to 1235 cm^{-1} compared to the other tested structures. We speculate that the branched morphology and the nanostaired surface of the spikes affected the two chemical functional groups of the semicrystalline polymer carrier (Figure 2a,c and Table 1). To further characterize the physical effect of the particle–polymer interphase interactions on PCL's crystalline planes, wide-angle X-ray diffraction (WAXD) was carried out. As shown in the Figure 2b,c, addition of ZnO nanoparticles within the fibrous polymer matrix led to sharpening of the PCL reflection planes, suggesting the variation in crystalline polymer domain sizes compared to pristine PCL nanofibers (4.2 Å).[22] This reflection displacement was more intense in substrates containing branched particles [displacement to the plane (110) (3.75 Å)], confirming the hypothesis that protrusions of the branched particles altered the PCL's overall crystallinity.

These results are in good agreement with the previous observations, pointing out that the branched ZnO nanoparticles induced crystallization in nylon-based composites.[23]

The mechanical properties of the composite fibers were assessed through the uniaxial tensile test to investigate the effect of the particles on the ultimate strength and the Young's modulus of the fibers. Figure 3a demonstrates that the incorporation of 1% (w/v) branched particles into polymer network led to a significant enhancement of the ultimate strength of the pristine PCL from 1.2 MPa to 1.9 MPa in the branched composite. A similar observation was reported in computational and experimental studies that demonstrated an improvement of bulk polymer properties due to the introduction of branched nanomaterials.[24] The trend is further evident considering the Young's modulus of the structures which drastically increased from 7 MPa for pristine PCL to ~13 MPa for the composite containing 1% branched ZnO ($p < 0.33$, Figure 3b). However, the addition of 3 and 5% (w/v) ZnO particles did not further reinforce the PCL structure but introduced weak point in the polymer network.[25]

The geometry of the branched particles and the rose-like constructs formed after their incorporation within the polymeric
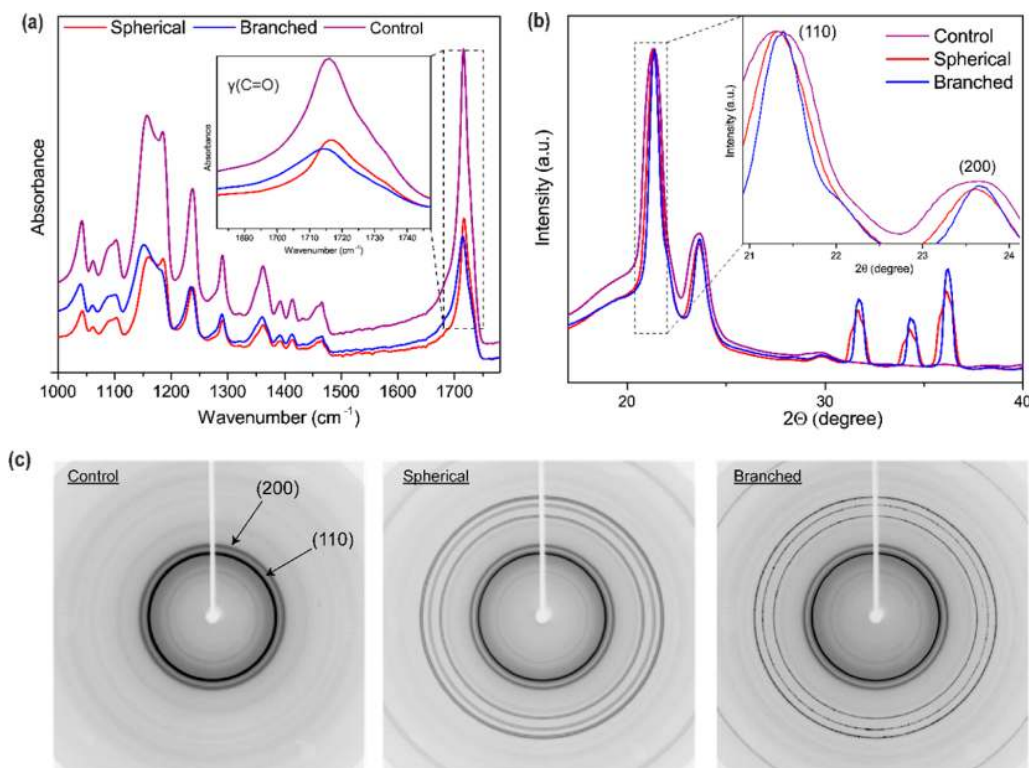

Figure 2. Chemical and physical characterization of fibrous composite scaffolds. (a) Fourier transformer infrared spectroscopy (FTIR) spectra of the tested fibers. The inset within the graph highlights the carbonyl stretching peaks. (b) Wide-angle X-ray diffraction (WAXD) showing the effect of the ZnO nanoparticles on the carrier polymer (PCL) (110) and (200) crystal planes. The inset demonstrates that the incorporation of ZnO induces narrowing of the crystal planes, correlating with an enhanced crystallization, compared to the control (purple). (c) Two-dimensional WAXD images show the effect of ZnO nanoparticles on the reflection banding arc's annotated within with arrows.

Table 1. FTIR Peaks of Interest within Tested Conditions

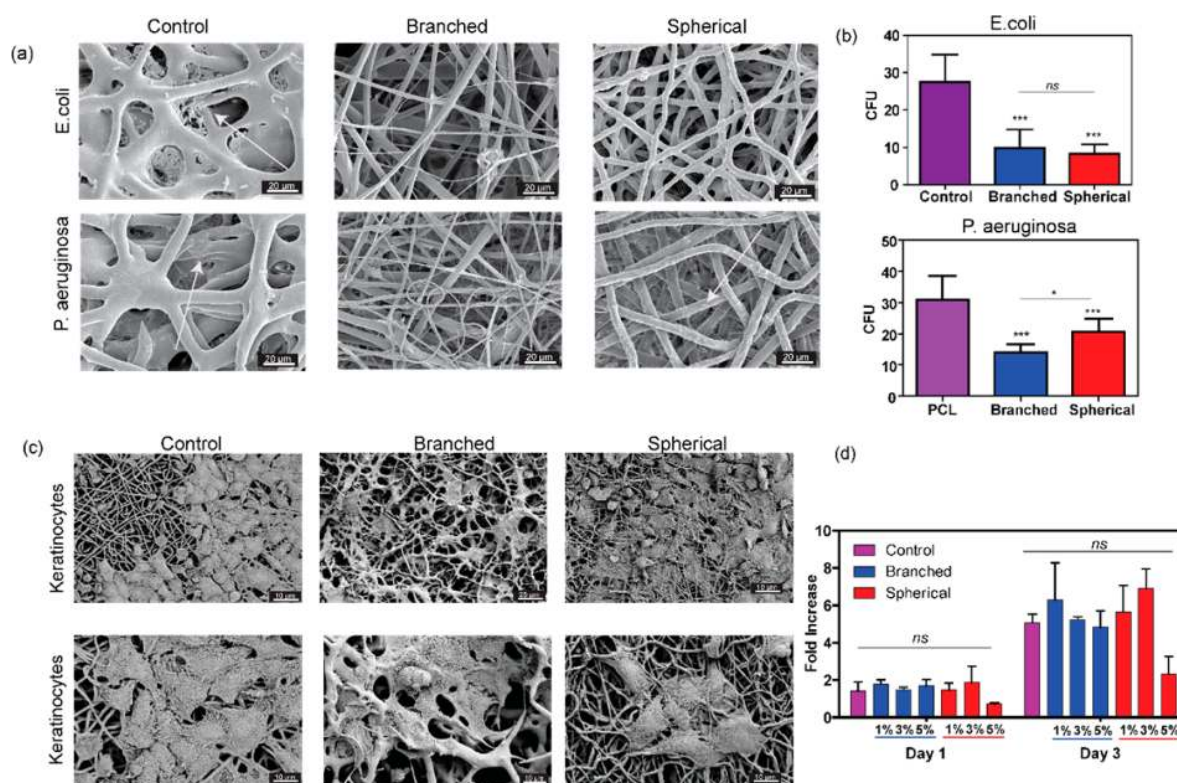| characteristic	control	spherical	branched
C–O and C–C stretching in the amorphous phase V_{am}	−1156 cm^{-1}	−1159 cm^{-1}	−1152 cm^{-1}
symmetric COC stretching V_s (COC)	−1185 cm^{-1}	−1185 cm^{-1}	
asymmetric COC stretching V_{as} (COC)	−1238 cm^{-1}	−1238 cm^{-1}	−1235 cm^{-1}
carbonyl stretching ν(C=O)	−1716 cm^{-1}	−1716 cm^{-1}	−1714 cm^{-1}
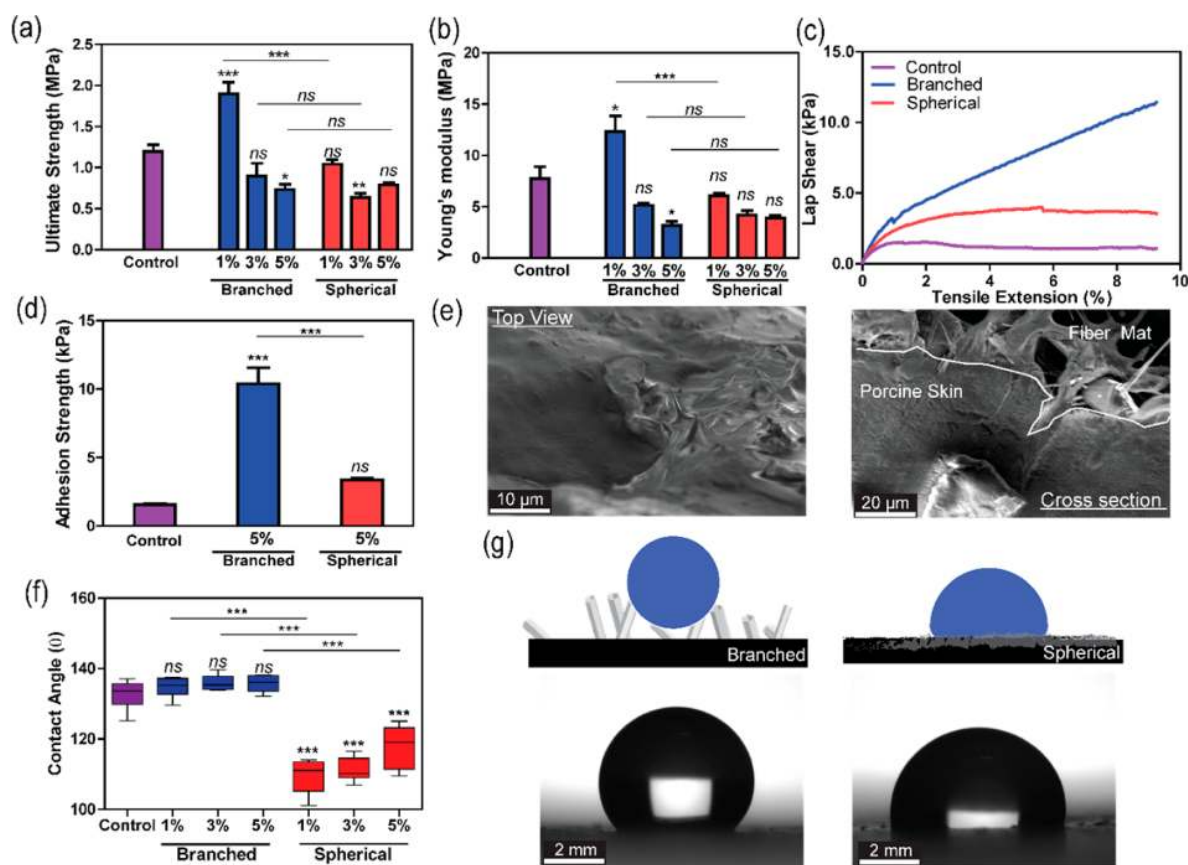
Figure 3. Mechanical and surface characterization of the nanocomposite structures. (a) Comparison of ultimate strength among the control sample (PCL), branched, and spherical composite scaffolds. The reports of statistical analysis placed directly on top of the bars refer to the comparison of the sample with the control (pristine PCL). The comparison between different samples is shown by lines. (b) Comparison of constructs' Young's modulus. (c) Representative lap shear curves of scaffolds sandwiched between porcine skins. (d) Comparison of the adhesion strength of different composite structures (data is derived from lap shear tests with porcine skin). (e) Representative SEM images from top and cross-sectional view of a branched composite material after failure during lap shear test. (f) Measurements of contact angle between a deionized water drop and the material surfaces. (g) Schematic illustration of fibrous structures wetting behavior (top). coupled with optical imaging analysis (bottom) ($n = 4$ for ultimate strength and Young's modulus data, $n = 3$ for adhesion strength data, and $n = 6$ for contact angle data, *: $P < 0.33$, **: $P < 0.002$, ***: $P < 0.001$).

membranes could facilitate the physical interlocking and penetration to soft substrate (such as tissues) to improve the adhesive properties. Surface topography can indeed play an important role in the adhesion strength between substrates and skin. In addition to the penetration of the spike of the rose-like substrates into skin, their high surface area may also positively contribute to the adhesion strength.

To prove our hypothesis, the electrospun fibers were sandwiched between two pieces of porcine skin and a uniform force with a 150 g weight was applied for 1 min. The use of the 5% (w/v) composite substrates in the adhesion tests was to note the effect of particle shape, on adhesion strength. We expected that the highest particle concentration would exhibit the most distinct difference. Samples were then subjected to lap shear test. Results showed that the rose stem-like composites containing 5% branched particles had significant higher adhesive properties (10.4 MPa) as compared to those containing 5% spherical particles (3.3 MPa) and pristine PCL (1.6 MPa) ($p < 0.001$ Figure 3c,d). SEM images from the interface of the porcine skin and the fiber mat with branched nanoparticles indicated the penetration of the spikes of branched particles into the porcine skin. Therefore, the increased adhesive strength might be due to the physical between topographically heterogenous electrospun fibers and the porcine skin (Figure 3e).

The variations in surface composition and architecture affect interfacial properties including the contact angle. The contact angle (CA) measurements on the scaffolds surface were performed to evaluate their wettability and hydrophilic/hydrophobic properties (Figure 3f). Pristine PCL was hydrophobic and showed a nonwetting regime (CA ∼ 130°). The incorporation of spherical particles slightly reduced the CA, improving the wetting regime of the PCL structure. In contrast, the branched composites showed higher CA, increasing the overall hydrophobicity of the fibrous constructs. The similarity between the contact angle of pristine PCL and rose-like structures might be due to coating of PCL on the surface of the spikes. SEM images suggested the presence of a thin layer of PCL on the surface of the spikes (Figure S2).

The antibacterial properties of ZnO nanoparticles have been previously shown and used for various medical applications.[26] To assess the antibacterial potency of the fabricated hybrid scaffolds, we used the lowest ZnO concentration (1% w/v). Substrates containing 1% (w/v) branched particles were seeded with prokaryotic microorganisms (*E. coli* and *P. aeruginosa*). Data reported in Figure 4a,b showed poor adhesion and proliferation of both tested microorganisms on ZnO composite fibrous scaffolds. Moreover, the reduction of the biofilm formation as compared to pristine PCL, confirmed that antibacterial properties

Figure 4. Characterization of the antimicrobial and biological properties of the composite scaffolds. (a) Representative SEM images of control (PCL), branched, and spherical samples after 24 h incubation with *E. coli* (top) and *P. aeruginosa*. (bottom) (b) Number of colony forming units (CFU) over the samples after 24 h incubation with *E. coli* (top) and *P. aeruginosa* (bottom). The arrows are showing the presence of bacteria on the surface of the nanofibers. (c) Representative SEM images of keratinocytes attachment to control, branched, and spherical composite scaffolds. (d) Metabolic activity of HACATs assessed by PrestoBlue assay after 1 and 3 days of culture over pristine PCL compared with ZnO nanocomposites with different concentrations (1, 3, 5%) of branched and spherical ZnO nanoparticles. ($n = 7$ for antimicrobial tests, $n = 5$ for metabolic activity tests, *: $P < 0.33$, **: $P < 0.002$, ***: $P < 0.001$).

were preserved following incorporation of the ZnO branched nanoparticles into the PCL electrospun fiber. The observed behavior might be due to the difference between the surface topography of substrates containing spherical and branched particles. In addition, the exposure of the ZnO nanospikes might have also contributed to the enhanced antibacterial activity.

Cells attachment on pristine PCL and ZnO containing fibrous substrates containing 5% (w/v) of particles was assessed by seeding human keratinocytes on the substrate. After 48 h, cells were fixed and imaged by SEM (Figure 4c). The images demonstrated a high cell attachment to fibrous scaffolds. The in vitro biocompatibility of fabricated scaffolds was further assessed by measuring the metabolic activity of the cells cultured on scaffolds using a PrestoBlue assay after 1 and 3 days (Figure 4d). Results showed that the branched ZnO particles do not induce any cytotoxic effects after incorporation within PCL mats. On the other hand, the scaffolds containing 5% (w/v) of spherical particles showed slight inhibitory effects on cellular growth. Considering the reduced bacteria growth and improved cellular growth, the engineered rose-like constructs may be an interesting candidate for regenerative applications susceptible to infection.

In conclusion, we have developed a PCL-based fibrous nanocomposite system embedded with spherical or branched ZnO nanoparticles. The focus of the work is to shed light on the difference in characteristics of composite substrates where the particles are exposed and not embedded within the polymeric fibers. However, the difference in particle size could also contribute to some of the observed differences in the properties of the fabricated composite substrates. Incorporation of the branched particles resulted in the formation of rose stem-like thorns. These geometric features resulted in enhanced mechanical properties and adhesion strength to soft tissue. The lower surface area of the branched ZnO nanoparticles in the electrospun fibers also led to higher biocompatibility as well as reduced antimicrobial activity. Therefore, at low concentrations of branched ZnO particles, the rose stem-like engineered constructs can be appropriate candidates for regenerative applications susceptible to infection as they support cellular growth and reduce bacterial adhesions.

■ ASSOCIATED CONTENT

Ⓢ Supporting Information

The Supporting Information is available free of charge on the ACS Publications website at DOI: 10.1021/acs.nanolett.7b02929.

Materials and methods; scanning electron microscopy (supplementary Figures S1−S4); stress strain curves (supplementary Figure S5) supplementary references (PDF)

■ AUTHOR INFORMATION

Corresponding Authors

*E-mail: alik@bwh.harvard.edu. Phone: (617)-768-8395. Fax: (617)-768-8477.

*E-mail: atamayol@bwh.harvard.edu.
*E-mail: sshin4@partners.org.

ORCID ⊙

Michael J. Mitchell: 0000-0002-3628-2244
Yogendra Kumar Mishra: 0000-0002-8786-9379
Ali Khademhosseini: 0000-0002-2692-1524

Notes
The authors declare no competing financial interest.

■ REFERENCES

(1) Leijten, J.; Rouwkema, J.; Zhang, Y. S.; Nasajpour, A.; Dokmeci, M. R.; Khademhosseini, A. *Small* **2016**, *12*, 2130−2145.
(2) Li, D.; Xia, Y. *Adv. Mater.* **2004**, *16*, 1151−1170.
(3) Persano, L.; Dagdeviren, C.; Su, Y.; Zhang, Y.; Girardo, S.; Pisignano, D.; Huang, Y.; Rogers, J. A. *Nat. Commun.* **2013**, *4*, 1633.
(4) Najafabadi, A. H.; Tamayol, A.; Annabi, N.; Ochoa, M.; Mostafalu, P.; Akbari, M.; Nikkhah, M.; Rahimi, R.; Dokmeci, M. R.; Sonkusale, S.; Ziaie, B.; Khademhosseini, A. *Adv. Mater.* **2014**, *26*, 5823−5830.
(5) Goldberg, M.; Langer, R.; Jia, X. *J. Biomater. Sci., Polym. Ed.* **2007**, *18*, 241−268.
(6) Gopal, R.; Kaur, S.; Ma, Z.; Chan, C.; Ramakrishna, S.; Matsuura, T. *J. Membr. Sci.* **2006**, *281*, 581−586.
(7) Huang, Z.-M.; Zhang, Y. Z.; Kotaki, M.; Ramakrishna, S. *Compos. Sci. Technol.* **2003**, *63*, 2223−2253.
(8) Keledi, G.; Hari, J.; Pukanszky, B. *Nanoscale* **2012**, *4*, 1919−1938.
(9) Augustine, R.; Malik, H. N.; Singhal, D. K.; Mukherjee, A.; Malakar, D.; Kalarikkal, N.; Thomas, S. *J. Polym. Res.* **2014**, *21*, 347.
(10) Augustine, R.; Dominic, E. A.; Reju, I.; Kaimal, B.; Kalarikkal, N.; Thomas, S. *RSC Adv.* **2014**, *4*, 51528−51536.
(11) Augustine, R.; Dominic, E. A.; Reju, I.; Kaimal, B.; Kalarikkal, N.; Thomas, S. *RSC Adv.* **2014**, *4*, 24777−24785.
(12) Mishra, Y. K.; Kaps, S.; Schuchardt, A.; Paulowicz, I.; Jin, X.; Gedamu, D.; Freitag, S.; Claus, M.; Wille, S.; Kovalev, A.; Gorb, S. N.; Adelung, R. *Part. Part. Syst. Charact.* **2013**, *30*, 775−783.
(13) Jin, X.; Götz, M.; Wille, S.; Mishra, Y. K.; Adelung, R.; Zollfrank, C. *Adv. Mater.* **2013**, *25*, 1342−1347.
(14) Holken, I.; Hoppe, M.; Mishra, Y. K.; Gorb, S. N.; Adelung, R.; Baum, M. J. *Phys. Chem. Chem. Phys.* **2016**, *18*, 7114−7123.
(15) Mishra, Y. K.; Modi, G.; Cretu, V.; Postica, V.; Lupan, O.; Reimer, T.; Paulowicz, I.; Hrkac, V.; Benecke, W.; Kienle, L.; Adelung, R. *ACS Appl. Mater. Interfaces* **2015**, *7*, 14303−14316.
(16) Nie, L.; Gao, L.; Feng, P.; Zhang, J.; Fu, X.; Liu, Y.; Yan, X.; Wang, T. *Small* **2006**, *2*, 621−625.
(17) Antoine, T. E.; Hadigal, S. R.; Yakoub, A. M.; Mishra, Y. K.; Bhattacharya, P.; Haddad, C.; Valyi-Nagy, T.; Adelung, R.; Prabhakar, B. S.; Shukla, D. *J. Immunol.* **2016**, *196*, 4566−4575.
(18) Jin, X.; Strueben, J.; Heepe, L.; Kovalev, A.; Mishra, Y. K.; Adelung, R.; Gorb, S. N.; Staubitz, A. *Adv. Mater.* **2012**, *24*, 5676−5680.
(19) Zander, N. *Polymers* **2013**, *5*, 19.
(20) Han, T.; Yarin, A. L.; Reneker, D. H. *Polymer* **2008**, *49*, 1651−1658.
(21) Elzein, T.; Nasser-Eddine, M.; Delaite, C.; Bistac, S.; Dumas, P. *J. Colloid Interface Sci.* **2004**, *273*, 381−387.
(22) Wang, X.; Zhao, H.; Turng, L.-S.; Li, Q. *Ind. Eng. Chem. Res.* **2013**, *52*, 4939−4949.
(23) Ma, Y.-l.; Hu, G.-s.; Ren, X.-l.; Wang, B.-b. *Mater. Sci. Eng., A* **2007**, *460−461*, 611−618.
(24) Raja, S. N.; Olson, A. C. K.; Limaye, A.; Thorkelsson, K.; Luong, A.; Lin, L.; Ritchie, R. O.; Xu, T.; Alivisatos, A. P. *Proc. Natl. Acad. Sci. U. S. A.* **2015**, *112*, 6533−6538.
(25) Raja, S. N.; Luong, A. J.; Zhang, W.; Lin, L.; Ritchie, R. O.; Alivisatos, A. P. *Chem. Mater.* **2016**, *28*, 2540−2549.
(26) Amna, S.; Shahrom, M.; Azman, S.; Kaus, N. H. M.; Ling Chuo, A.; Siti Khadijah Mohd, B.; Habsah, H.; Dasmawati, M. *Nano-Micro Lett.* **2015**, *7*, 219−242.